NeuroImage 47 (2009) 148–156

Contents lists available at ScienceDirect

NeuroImage

journal homepage: www.elsevier.com/locate/ynimg

Resting-state functional connectivity in the human brain revealed with diffuse optical tomography

Brian R. White [a,b], Abraham Z. Snyder [a,c], Alexander L. Cohen [c], Steven E. Petersen [a,c,d,e], Marcus E. Raichle [a,c,d,f], Bradley L. Schlaggar [a,c,d,g], Joseph P. Culver [a,b,*]

[a] Department of Radiology, Washington University, St. Louis, MO 63110, USA
[b] Department of Physics, Washington University, St. Louis, MO 63130, USA
[c] Department of Neurology, Washington University, St. Louis, MO 63110, USA
[d] Department of Anatomy and Neurobiology, Washington University, St. Louis, MO 63110, USA
[e] Department of Psychology, Washington University, St. Louis, MO 63110, USA
[f] Department of Biomedical Engineering, Washington University, St. Louis, MO 63130, USA
[g] Department of Pediatrics, Washington University, St. Louis, MO 63110, USA

ARTICLE INFO

Article history:
Received 15 January 2009
Revised 12 March 2009
Accepted 20 March 2009
Available online 1 April 2009

ABSTRACT

Mapping resting-state networks allows insight into the brain's functional architecture and physiology and has rapidly become important in contemporary neuroscience research. Diffuse optical tomography (DOT) is an emerging functional neuroimaging technique with the advantages, relative to functional magnetic resonance imaging (fMRI), of portability and the ability to simultaneously measure both oxy- and deoxyhemoglobin. Previous optical studies have evaluated the temporal features of spontaneous resting brain signals. Herein, we develop techniques for spatially mapping functional connectivity with DOT (fc-DOT). Simultaneous imaging over the motor and visual cortices yielded robust correlation maps reproducing the expected functional neural architecture. The localization of the maps was confirmed with task-response studies and with subject-matched fc-MRI. These fc-DOT methods provide a task-less approach to mapping brain function in populations that were previously difficult to research. Our advances may permit new studies of early childhood development and of unconscious patients. In addition, the comprehensive hemoglobin contrasts of fc-DOT enable innovative studies of the biophysical origin of the functional connectivity signal.

© 2009 Elsevier Inc. All rights reserved.

Introduction

Optical neuroimaging has never lacked clinical potential, due to its ability to longitudinally and non-invasively monitor brain function. However, progress towards the bedside practice of methods to map brain function, such as functional near infrared spectroscopy (fNIRS), has been hindered by conceptual and technical limitations. One obstacle is that task-based neuroimaging, which is standard in cognitive neuroscience research, is generally ill-suited to clinical populations since they may be unable to perform any task. Recently in functional magnetic resonance imaging (fMRI), it was discovered that even during the absence of overt tasks, fluctuations in brain activity are correlated across functionally-related cortical regions (Biswal et al., 1995). Thus, the spatial and temporal evaluation of spontaneous neuronal activity has allowed mapping of these resting-state networks (RSNs) (Fox and Raichle, 2007). Translating these advances to optical techniques would enable new clinical and developmental studies. Yet, mapping spontaneous activity with fNIRS measurements presents significant challenges due to the obscuring influences of superficial signals, systemic physiology, and auto-regulation. In this paper, we develop three-dimensional diffuse optical tomography (DOT) (Zeff et al., 2007; Yodh and Chance, 1995; Joseph et al., 2006; Bluestone et al., 2001; Gibson et al., 2006) and linear regression techniques that, combined with correlation analysis, allow us to isolate functional maps from resting-state measurements and demonstrate the feasibility of functional connectivity DOT (fc-DOT).

Low frequency fluctuations in cerebral hemodynamics have been detected by NIRS (Obrig et al., 2000; Elwell et al., 1999). However, as the optical signal is a mixture of hemodynamics within the scalp, skull, and brain, it is particularly susceptible to artifacts from systemic changes. Such fluctuations have been found to obscure functional responses in fNIRS studies (Jasdzewski et al., 2003; Boden et al., 2007). In addition, their frequency components overlap those of RSNs. As with fc-MRI, these systemic contributions must be removed to observe the underlying spatial maps of the brain networks. In part because fNIRS has traditionally had difficulty in separating different physiologic contributions, previous resting-state

* Corresponding author. Campus Box 8225, 4525 Scott Ave. – East Building, St. Louis, MO 63110, USA. Fax: +314 747 5191.
E-mail address: culverj@wustl.edu (J.P. Culver).

1053-8119/$ – see front matter © 2009 Elsevier Inc. All rights reserved.
doi:10.1016/j.neuroimage.2009.03.058

studies have focused on investigating the correlation between the measured signal and systemic physiological variables (Rowley et al., 2007; Reinhard et al., 2006; Katura et al., 2006; Franceschini et al., 2006). While such experiments have yielded interesting results, including some within the clinical setting (Schroeter et al., 2005), they have not moved beyond temporal analysis to the study of spatial correlations and neural connectivity. fNIRS also suffers from spatial limitations. Low spatial resolution (>3 cm) may average out any underlying spatial correlation structure. In addition, an fNIRS study to detect RSNs requires a field-of-view greater than typically available in order to cover both correlated and uncorrelated (e.g., control) brain regions.

While there are multiple challenges, both physiological and methodological, to the development of fc-DOT systems, their successful creation would open up new approaches to the research of resting-state physiology. The discovery of functional connectivity (fc-MRI) has led to its use as an important tool throughout neuroimaging research (Fox and Raichle, 2007), including insights into childhood brain development (Fair et al., 2007; Fransson et al., 2007; Fair et al., 2008). Recent fc-MRI studies have found RSNs that are altered in patients with depression (Greicius et al., 2007), Alzheimer's disease (Greicius et al., 2004), and Tourette syndrome (Church et al., 2009). However, important brain-injured populations, such as intensive care patients, cannot be easily transported to fixed scanner environments. The portability and wearability (Obrig and Villringer, 2003) of fc-DOT systems could allow significant applications in populations that are not amenable to traditional functional neuroimaging, such as hospitalized patients and young children.

In addition, DOT provides a more comprehensive assessment of hemodynamics and metabolism than the blood oxygenation level-dependent (BOLD) signal, due to BOLD's complicated connection to the underlying neurovascular coupling (Raichle and Mintun, 2006; Heeger and Ress, 2002). While relying on the neurovascular response in much the same manner as BOLD-fMRI, DOT can measure changes in oxy - (HbO_2), deoxy - (HbR), and total hemoglobin (HbT) (the BOLD contrast is mostly sensitive to HbR) at a much higher sampling rate (at least 10 Hz, compared to ~0.5 Hz with fMRI) (Steinbrink et al., 2006). This enhanced view of brain activity is especially important when the neurovascular coupling is either unknown (as in infants) (Born et al., 1998; Morita et al., 2000; Colonnese et al., 2008) or altered (as with brain injury) (Fujiwara et al., 2004; Bonakdarpour et al., 2007; Zou et al., 2005; Iadecola, 2004; D'Esposito et al., 2003).

To address our goal of fc-DOT mapping, we developed a DOT system with extended field-of-view that provides unique simultaneous 3D imaging of distributed cortical regions covering both the visual and motor cortices with high resolution. These spatial techniques are complemented by linear regression methods that remove global superficial signals and correlation analyses to map spontaneous brain activity patterns. We judge the success of fc-DOT by our ability to obtain spatial correlations maps based on local physiology that match the fc-MRI literature and our own subject-matched fc-MRI experiments. Functional connectivity was first demonstrated by BOLD-fMRI detecting low-frequency variations in the motor cortex during the resting state (Biswal et al., 1995). fc-MRI's original validation was that the resulting spatial correlations corresponded with the brain's functional architecture as mapped by task-induced responses. Previous fc-MRI studies have also demonstrated that the motor and visual cortices constitute largely independent functional networks, each exhibiting high levels of inter-hemispheric correlation (De Luca et al., 2006; Damoiseaux et al., 2006). We, thus, expect resting-state analysis of seed regions found from a sensory task-response study to reveal that sensory network, while the other sensory network will provide a control that should be uncorrelated. These studies aim to establish the utility of DOT for functional connectivity analysis.

Methods

Protocol

Healthy adult subjects were recruited (4 female and 1 male, ages 24–27). Informed consent was obtained prior to both DOT and MRI scanning. The protocol was approved by the Human Research Protection Office of the Washington University School of Medicine. Stimulus studies were performed to locate the motor and visual cortices. The visual cortex was stimulated using pseudorandom blocks of right and left lower visual quadrant reversing checkerboard grids (10 Hz reversal on 50% gray background, 10 s on and 20 s off). The sensorimotor cortex was stimulated with pseudorandom blocks of right and left finger tapping (self-paced at about 3 Hz, 10 s on and 20 s off). For resting-state analysis, a 50% gray screen with a crosshair was viewed (in 5 min blocks for 10 or 15 min total).

DOT imaging

Subjects were seated in an adjustable chair facing a 19" LCD screen at 70 cm viewing difference. DOT imaging arrays were placed over the visual (24 sources, 28 detectors, Fig. 1a) and sensorimotor (24 sources, 18 detectors, Fig 1b) cortices and held in place with hook-and-loop strapping. The position of the pads relative to the nasion and inion was measured to establish repeatable positioning. Each source position is illuminated by light emitting diodes at two wavelengths (750 nm and 850 nm) to enable hemoglobin spectroscopy. Detector positions are recorded by avalanche photodiodes (Hamamatsu C5460-01) and dedicated 24-bit analog-to-digital converters (MOTU HD192), which enable high dynamic range ($>10^6$) and low crosstalk ($<10^{-6}$). The dynamic range allows the detection of light from multiple source detector distances: separations of first-(13 mm), second-(30 mm), third-(40 mm), and fourth-nearest neighbors (48 mm).

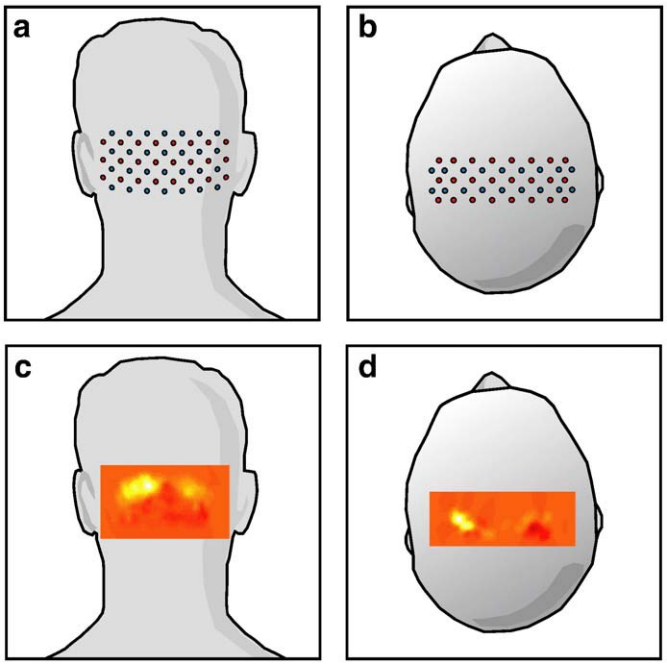

Fig. 1. Our DOT imaging system with functional responses. (a) Schematic of the visual cortex imaging pad (24 sources, red, and 28 detectors, blue). (b) Schematic of the motor cortex imaging pad (24 sources, red, and 18 detectors, blue). (c) A left visual cortex response (ΔHbO_2), posterior coronal projection of a cortical shell. (d) A motor cortex response (ΔHbO_2), superior axial projection of a cortical shell.

Data were converted to log-ratio and high-pass filtered (0.02 Hz for stimulus data, 0.009 Hz for resting-state data) to remove long-term drift. An average of all 1st-nearest-neighbor measurements (13 mm separation, sampling predominantly scalp and skull) on each pad was constructed as an estimate of global and superficial signals (Zeff et al., 2007; Saager and Berger, 2005). This signal was then regressed from all measurements within each pad. After a low-pass filter (0.5 Hz) removed residual pulse signals, the time traces were used for image reconstruction.

Prior to inversion, channels with high standard deviation (>7.5%) within a given run were removed from the reconstruction to reduce image noise due to such artifacts as optode motion. A typical run kept 98.9% of 1st-nearest-neighbors, 96.4% of 2nd-nearest-neighbors, 59.1% of 3rd-nearest-neighbors, and 19.0% of 4th-nearest-neighbors. So, the reconstruction is primarily dependent on 1st- and 2nd-nearest-neighbors, while 3rd-(and to a lesser extent 4th-) nearest-neighbors provide additional depth information when possible. Note that while a time trace of the average across channels of all 1st-nearest-neighbor pairs was removed during the global signal regression, the individual 1st-nearest-neighbor channels retain variance after this regression and are used during the reconstruction.

A two-layer head model was used with finite-element software (NIRFAST) (Dehghani et al., 2003) to generate a light-sensitivity matrix of the DOT arrays. The inverted sensitivity matrix converts time series measurement data into a series of three-dimensional images of differential absorption for each wavelength. Changes in the concentrations of HbO_2 and HbR were then obtained using their extinction coefficients. HbT was obtained as a simple sum of the two hemoglobin species. For further reconstruction details, see our earlier publication (Zeff et al., 2007). A cortical shell (1 cm thickness) was selected and all images shown are projections of this shell (Visual: posterior coronal view, Motor: superior horizontal view, Figs. 1c, d).

fc-DOT analysis

Functional response images were obtained by block-averaging each subject's trials and temporally averaging (5 s) around the peak hemodynamic response. For each of the four regions of interest (left/right visual and left/right motor cortices) and for each subject, a 1 cm^3 volume was chosen as a seed region for correlation analysis. Resting-state images were low-pass filtered (0.08 Hz). The resting-state time traces from within each seed volume were averaged to create a seed signal, and correlation coefficients were calculated between the seed signal and every other voxel in the field-of-view of both imaging pads (see Correlation statistics).

fMRI acquisition and analysis

For comparison, we scanned one subject with fc-MRI. fMRI data were acquired on a Siemens 3 T MAGNETOM Trio scanner (Erlangen, Germany). The session included two structural scans: a T1-weighted MP-RAGE sequence (TE = 3.08 ms, TR(partition) = 1000 ms, flip angle = 8°, 176 slices with 1 × 1 × 1 mm voxels) and a T2-weighted turbo spin-echo image (TE = 84 ms, TR = 6.8 s, 32 slices with 1 × 1 × 4 mm voxels). Resting-state fMRI was performed using a BOLD-sensitive asymmetric spin-echo echo-planar sequence (TE = 27 ms, flip angle = 90°, in-plane resolution 4 × 4 mm). Whole-brain EPI volumes of 40 contiguous, 4 mm-thick axial slices are obtained every 2.5 s. For each resting-state acquisition run, the subject viewed a small crosshair on the screen while 128 consecutive frames were acquired (320 s). Four resting-state runs were acquired (~20 min total). Preprocessing removed motion and systematic intensity differences. Images were registered to an atlas, resampled to 3 mm cubic voxels, and spatially smoothed. Each voxel's time course was temporally band-pass filtered (0.009–0.08 Hz) and linear regression removed sources of spurious correlations: signals from head motion, the whole-brain average, the ventricles, and white matter. Seed regions (9 mm radius spheres) were chosen through direct viewing of anatomy in Analyze (http://www.analyzedirect.com/), choosing regions over superficial central sulcus and extra-striate cortex. The BOLD signal within each seed volume was then used to make a correlation map in the same manner as with DOT (see Correlation statistics). For visualization, correlation coefficients were mapped to the fiducial surface segmentation in Caret (http://brainmap.wustl.edu/caret) (Van Essen et al., 2001).

Correlation statistics

The following random-effects analysis was conducted for each contrast separately. Correlations between time traces were calculated using the Pearson correlation coefficient, *r*, which is displayed in the correlation images. To examine the significance of the inter-hemispheric correlations within the motor and visual networks as measured with fc-DOT, we constructed two sets of inter-hemispheric *r*-values (motor-to-motor and visual-to-visual). Each set contained seven values: one *r*-value each per scan session. A third set of residual background correlation coefficients was created from the motor-to-visual *r*-values (all four possible seed-to-seed correlations averaged to one *r*-value per subject). The null hypothesis was then that each inter-hemispheric set was indistinguishable from the background set. This

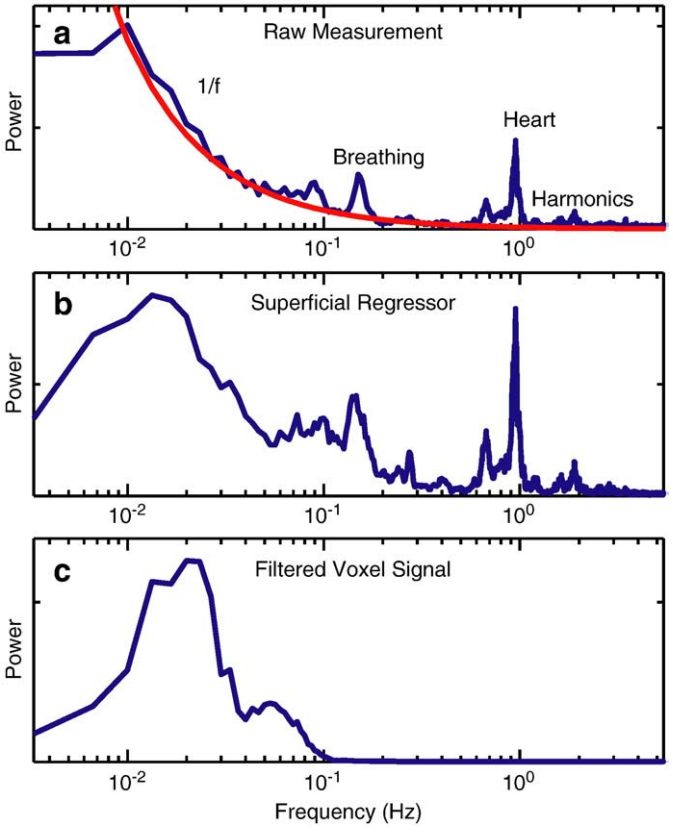

Fig. 2. Power spectra of resting-state DOT signals (ΔHbO_2) (a) Spectral power of a single 2nd-nearest-neighbor resting-state time trace, sampling both brain and superficial tissues, before the application of any filters (5 min, subject 2). The low-frequency components follow a 1/f curve (red), and there are peaks at the respiratory (0.16 Hz) and cardiac rates (0.95 Hz). (b) Spectral power of the superficial regressor derived from all first-nearest-neighbor measurements in the visual pad. These systemic low-frequency fluctuations are removed from the data prior to performing functional connectivity mapping. (c) Spectral power of a filtered imaged signal (5 min from a single voxel under the measurement in (a)). This remaining spectral power within the desired frequency range is used to perform fc-DOT. All traces have been smoothed with a moving average filter, width 5 points.

hypothesis was tested with a paired (within subject) Student's *t*-test. The *t*-statistics were converted to *p*-values using the right-tail of the distribution (i.e., we expected positive correlation within each network).

Results

With our extended DOT system, we simultaneously imaged with DOT arrays placed over the visual and motor cortices (Figs. 1a,b). Task paradigms were performed to locate the motor and visual cortices within each subject, yielding functional responses with high contrast-to-noise (Figs. 1c, d).

Spectral analysis of resting-state measurements (5 min) showed 1/f components as well as distinct peaks attributable to cardiac (0.75–1 Hz) and respiratory (0.1–0.3 Hz) frequencies (Fig. 2a shows an example Fourier transform from subject 2). Since the temporal sampling rate of the DOT system (10.8 Hz) is much higher than that of typical fMRI (~0.5 Hz), these physiologic confounds were not aliased into lower frequency bands. However, there are also vascular confounds from systemic auto-regulation that occur within the same frequency range as RSN correlations. Using a subset of signals that have minimal penetration into the brain, we constructed measures of each pad's scalp hemodynamics (Fig. 2b). Every channel had the superficial/global signal removed by regression and was band-pass filtered. These obscuring signals constituted on average 37% of deeper channels' power in the low-frequency functional connectivity regime. Three-dimensional image reconstructions of these source–detector measurements then allowed the localization of brain physiology. This processing was designed to result in voxel time courses that are unobscured by systemic confounds (Fig. 2c). The goal was to distinguish between systemic and local physiologic sources of low-frequency variations, allowing us to perform correlation mapping solely on the latter.

With the aid of the functional responses, seeds regions (1 cm^3) were chosen for use in correlation analysis (Visual: Figs. 3a,d, Motor: Figs. 3g, j; this figure shows data from subject 1). From each seed region, the time traces of ΔHbO_2, ΔHbR, and ΔHbT during resting-state brain activity were extracted. We then determined the correlation coefficient between these seed regions and every other cortical voxel's time course. For the visual cortex seeds, the images show that each seed region was correlated with the surrounding

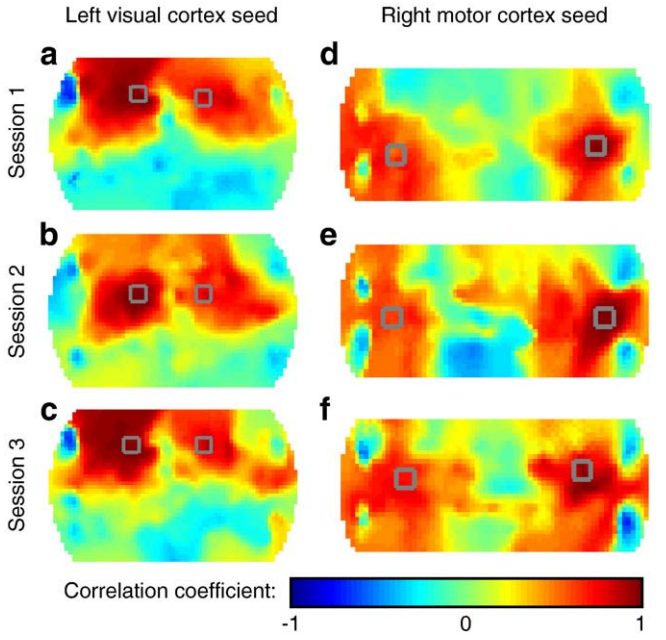

Fig. 4. Repeatability of fc-DOT over multiple imaging sessions (subject 1, ΔHbR). Seed boxes are shown in gray. Images from different sessions are not co-registered. (a–c) Correlation maps within the visual cortex from the left visual cortex seed. (d–f) Correlation maps within the motor cortex from the right motor cortex seed. Note the similarity in the patterns in each session (with slight linear translations between days).

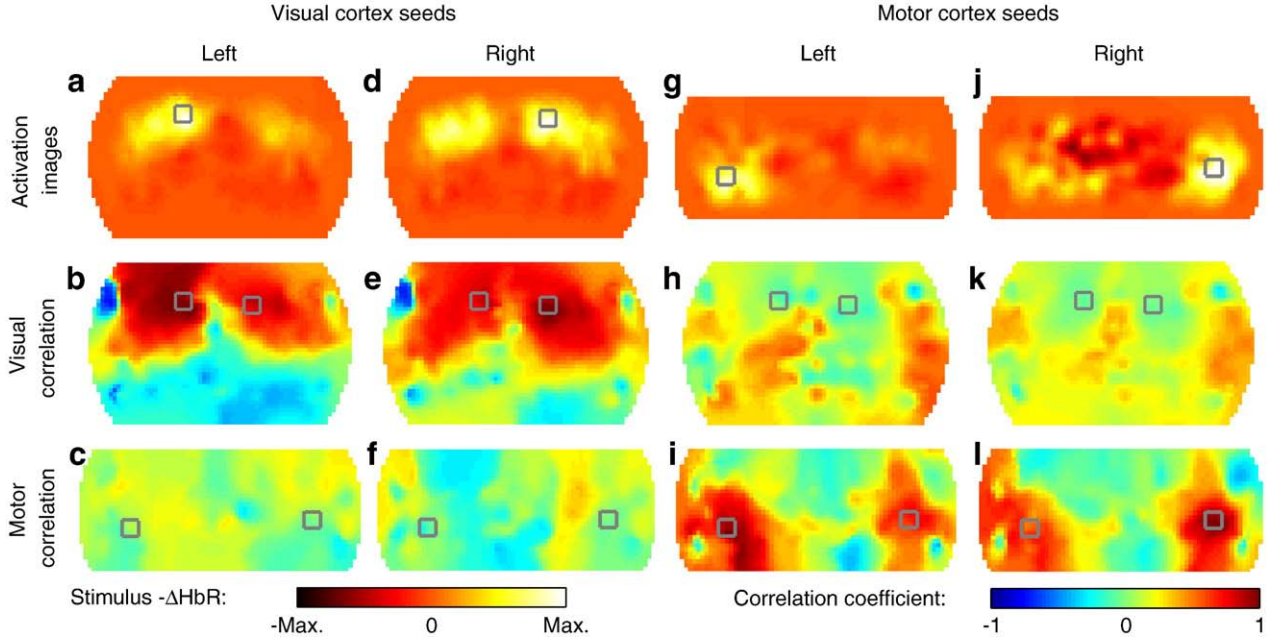

Fig. 3. fc-DOT using correlation analysis (ΔHbR, subject 1, session 1). (a) A functional response in the left visual cortex. There is a decrease in HbR with high contrast-to-noise. The response is scaled to its maximum contrast (scale reversed so decreases in HbR are positive contrast). The left visual cortex seed is defined by the gray box. (b) Correlation map in the visual cortex using the left visual cortex seed. There is correlation with both hemispheres of the visual cortex, but not with the lower region of the pad. Boxes for both right and left seed regions are shown. All correlation images scale from $r = -1$ to 1. (c) Correlation map in the motor cortex using the left visual cortex seed. The correlation throughout the field-of-view is low. Both right and left motor seed boxes are shown for reference. (d–f) fc-DOT using the right visual cortex seed. Note the similar pattern to the left visual seed. (g)–(i) fc-DOT using the left motor cortex seed. Note the high inter-hemispheric correlation in the motor cortex, but lack of any high correlations with the visual cortex. (j–l) fc-DOT using the right motor cortex seed. Note the similar pattern to the left motor seed.

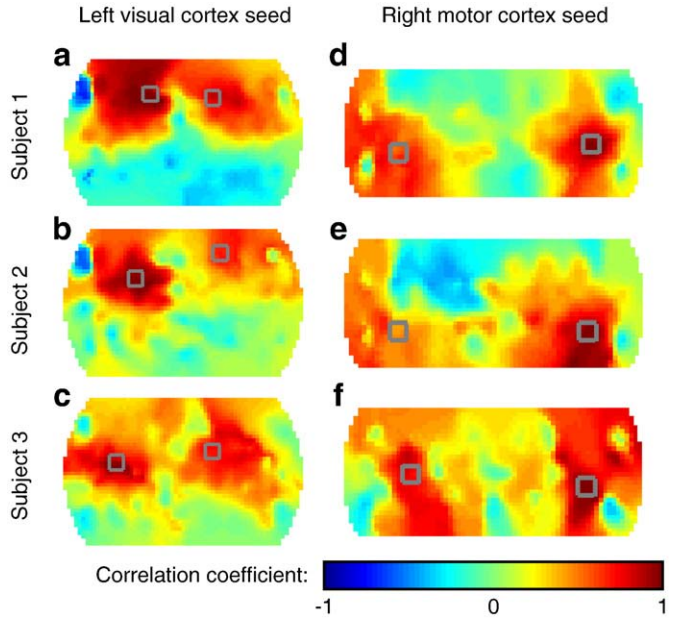

Fig. 5. Robustness of fc-DOT mapping in multiple subjects (ΔHbR). Seed boxes are shown in gray. For subject 1, session 1 is shown. (a–c) Correlation maps within the visual cortex from the left visual cortex seed. (d–f) Correlation maps within the motor cortex from the right motor cortex seed. All subjects have of high inter-hemispheric connectivity in both networks.

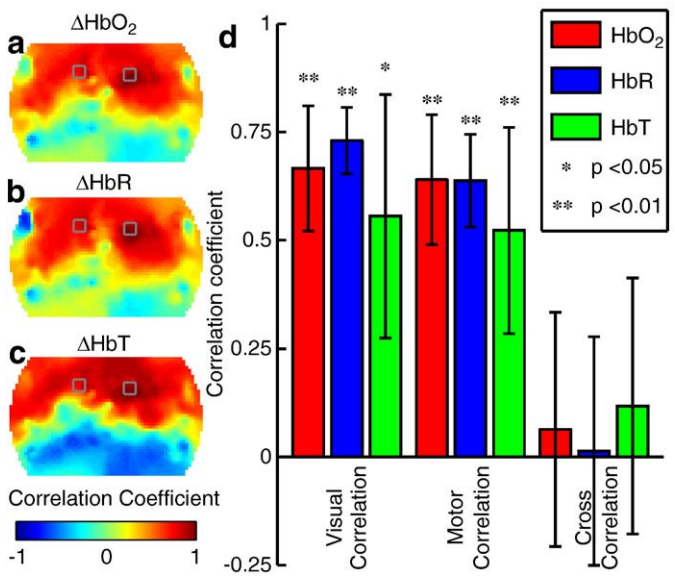

Fig. 7. fc-DOT analysis with all three hemoglobin contrasts (ΔHbO2, ΔHbR, and ΔHbT). (a–c) Visual correlation maps from the right visual cortex seed for each of the three contrasts (subject 1, session 1). Seed regions are shown in gray. The maps for ΔHbO_2 and ΔHbR are very similar. The map for ΔHbT is less localized, has more regions of negative correlation, and is more variable from subject-to-subject. (d) Correlation coefficients across multiple subjects and days for all three contrasts (mean and standard deviation). The *p*-value comparing each inter-hemispheric correlation to the visual-to-motor correlation within each contrast is shown. Visual and motor networks are significantly correlated with all three contrasts, while there is little correlation between the visual and motor cortices.

cortex, the more lateral cortex, and the contralateral cortex (Figs. 3b, e). In addition, the visual cortex seeds were uncorrelated with the motor cortex (Figs. 3c, f). Similarly, correlation mapping for the motor cortex seeds resulted in symmetrical correlation profiles with the contralateral motor cortex (Figs. 3i, l), but not within the visual cortex (Figs. 3h, k).

We investigated the repeatability of the fc-DOT results through repeated mapping of the same subject. Correlation analysis from three sessions showed that the patterns were qualitatively similar over multiple days (Fig. 4). In addition, robustness was assessed with images acquired across a total of five subjects, all showing comparable connectivity patterns (Fig. 5 shows three subjects). The average of the functional connectivity maps from all seven sessions shows inter-hemispheric correlations in both the motor and visual networks with low crosstalk between the two networks (Fig. 6).

fc-DOT analysis was repeated with all three hemodynamic contrasts. All the resulting correlation maps had the same pattern of inter-hemispheric correlations (Figs. 7a–c show examples from subject 1). However, ΔHbT shows qualitatively lower spatial localization and more areas of negative correlation. In order to assess the statistical significance of the correlations within the visual and motor cortices, we repeated our fc-DOT imaging and correlation analysis across seven scanning sessions (five subjects total, three sessions in subject 1). These data were evaluated with a random-effects model using the seed-to-seed correlation coefficients from all three hemodynamic contrasts. The group sets of inter-hemispheric correlation coefficients were compared against the set of visual-to-motor correlation coefficients within each contrast (Fig. 7d). The correlations were most robust in ΔHbR (Visual:

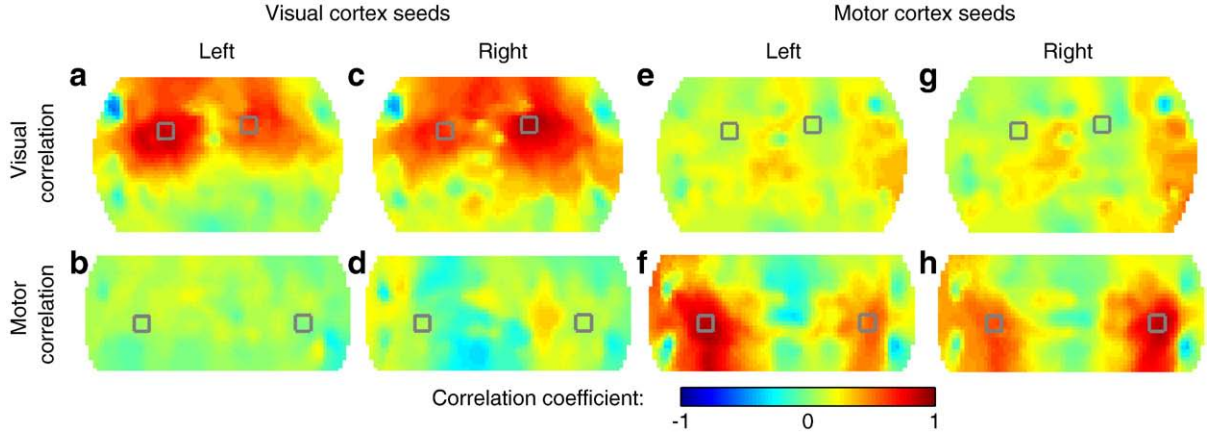

Fig. 6. Multi-session of average of all fc-DOT correlation maps (ΔHbR). (a) Correlation map in the visual cortex using the left visual cortex seed. There is correlation with both hemispheres of the visual cortex, but not with the lower region of the pad. Boxes for both right and left seed regions are shown. All correlation images scale from $r = -1$ to 1. (b) Correlation map in the motor cortex using the left visual cortex seed. The correlation throughout the field-of-view is low. Both right and left motor seed boxes are shown for reference. (c, d) fc-DOT using the right visual cortex seed. Note the similar pattern to the left visual seed. (e–h) fc-DOT using the motor cortex seeds. Note the high inter-hemispheric correlation in the motor cortex, but lack of any high correlations with the visual cortex.

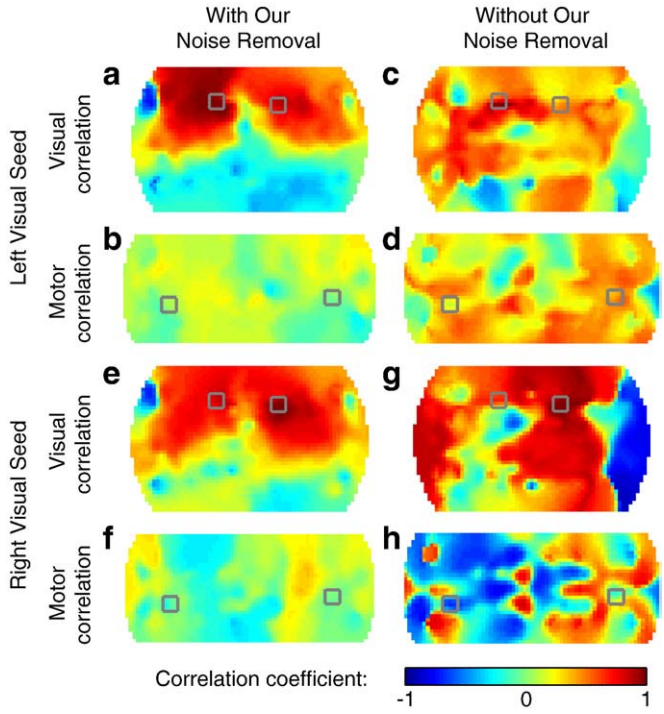

Fig. 8. fc-DOT with and without our regression and signal-to-noise reduction techniques (ΔHbR, subject 1, session 1). (a, b) Correlation maps in the visual and motor cortices using the left visual cortex seed with regression and noise removal. (The same images as Figs. 3b, c.) (c, d) Correlation maps using the left visual cortex seed without regression and noise removal. While this is the same raw data as (a) and (b), we now see global high correlations due to systemic confounds and artifact structure (possibly from coupling to optode motion) that obscures any underlying structure. Note the lack of any local correlation structure and the high correlations with the motor cortex. (e, f) Correlation maps using the right visual cortex seed with regression and noise removal. (The same images as Figs. 3e, f.) (g, h) Correlation maps using the right visual cortex seed without regression and noise removal. While this is the same raw data as (e) and (f), we now lack of the local correlation pattern seen in (e).

$p = 1.7 \times 10^{-4}$, Motor: $p = 9.4 \times 10^{-4}$) and were also significant in ΔHbO_2 (Visual: $p = 2.1 \times 10^{-3}$, Motor: $p = 4.1 \times 10^{-4}$). ΔHbT had the largest standard deviations and highest p-values, but still had statistically significant inter-hemispheric correlations (Visual: $p = 2.2 \times 10^{-2}$, Motor: $p = 7.1 \times 10^{-3}$). If, however, we do not remove channels with poor signal-to-noise and do not regress out superficial hemodynamic oscillations that allow us to localize neural activity, then the correlation p-values increase by two orders-of-magnitude (ΔHbO_2: Visual: $p = 0.08$, Motor: $p = 0.23$; ΔHbR: Visual: $p = 0.04$, Motor: $p = 0.12$; ΔHbT: Visual: $p = 0.17$, Motor: $p = 0.80$). The correlation maps created without signal-to-noise reduction are dominated by artifact structure due to corruption by measurements with poor signal-to-noise. In addition, the resulting maps have globally high

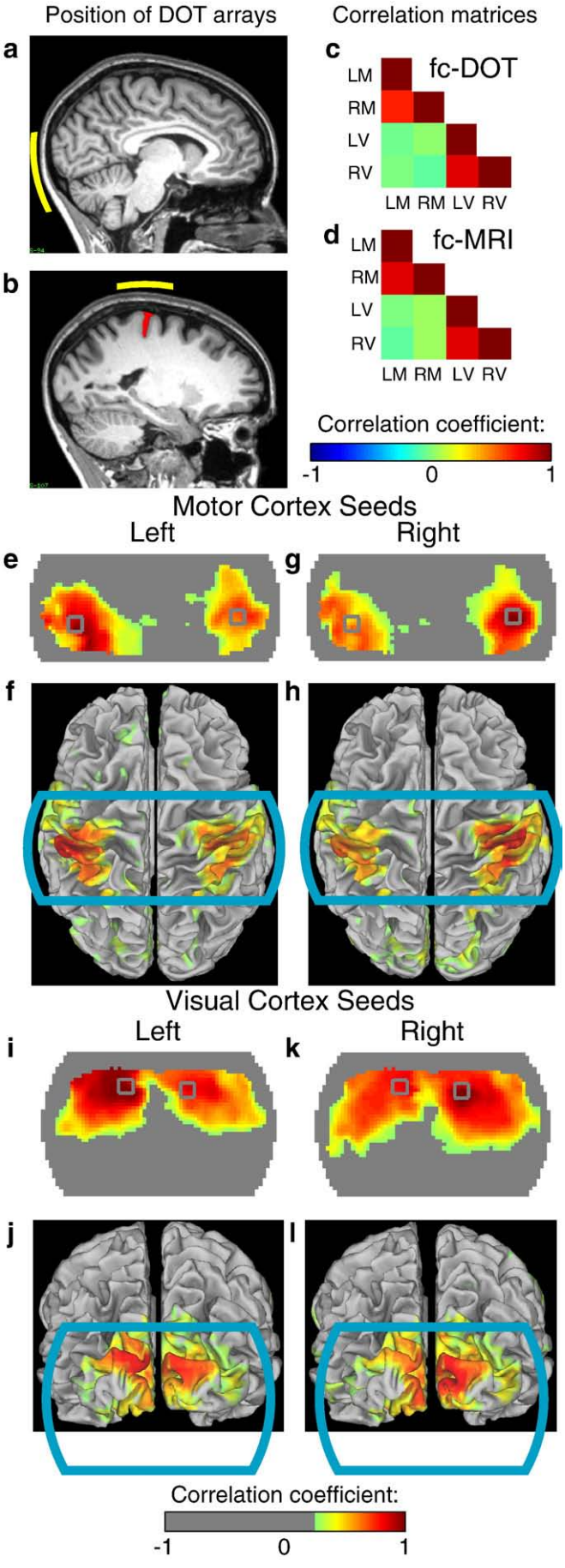

Fig. 9. Similarity of correlation maps from fc-DOT (subject 1, session 1) and fc-MRI (subject 1). (a) Sagittal slice (5 mm left of midline) from subject's anatomical MRI with schematic of the visual cortex DOT pad superimposed (yellow), showing its position over the visual cortex. (b) Sagittal slice (18 mm left of midline) from an anatomical MRI with schematic of the motor cortex DOT pad superimposed (yellow), showing its position over the central sulcus (red). (c) Cross-correlation matrix for all four seeds from fc-DOT imaging (LM: left motor cortex, RM: right motor cortex, LV: left visual cortex, RV: right visual cortex). Note the high inter-hemispheric correlations and low correlations between the motor and visual networks. (d) Cross-correlation matrix for all four seeds from fc-fMRI imaging. Note the similarity to the fc-DOT correlation matrix. (e) fc-DOT correlation map using the left motor cortex seed. (f) fc-MRI correlation map, dorsal view, using the left motor cortex seed. The DOT motor imaging pad's position is shown in cyan. (g, h) fc-DOT and fc-MRI (dorsal view) using the right motor cortex seed. (i, j) fc-DOT and fc-MRI (posterior view) using the left visual cortex seed. (k, l) fc-DOT and fc-MRI (posterior view) using the right visual cortex seed. Note the similarity of the fc-DOT and fc-MRI connectivity maps for all four seeds. The color scale has a threshold at $r = 0.25$.

correlations, showing that systemic physiology can obscure local variations. These maps do not localize neural activity or map functional connectivity (Fig. 8).

For further validation, the results of fc-DOT (subject 1, session 1) were compared against those obtained from the same subject with (non-simultaneous) fc-MRI. Measuring the position of the DOT imaging pads relative to external anatomic landmarks (inion and nasion) and locating these features in an anatomic MRI confirmed that the DOT imaging pads were interrogating the visual and motor cortices (Figs. 9a, b). The seed-to-seed correlation coefficients generated by fc-DOT analysis were similar to those from fc-MRI (Figs. 9c, d). Both correlation matrices show high inter-hemispheric visual (DOT: $r = 0.80$, fMRI: $r = 0.70$) and motor (DOT: $r = 0.68$, fMRI: $r = 0.79$) correlations. The motor-to-visual correlations were approximately zero with both methods (DOT: $r = -0.03 \pm 0.04$, fMRI: $r = 0.00 \pm 0.07$, mean and standard deviation). Correlation images were also generated with resting-state fMRI data and the results are qualitatively similar to those from fc-DOT in both the motor and visual cortices (Figs. 9e–l).

Discussion

We hypothesized that we would be able to measure functional connectivity within the visual and motor networks using DOT. From fMRI reports and from our fc-MRI studies, both networks exhibit high levels of inter-hemispheric correlation (De Luca et al., 2006; Damoiseaux et al., 2006). In addition, the motor and visual cortices are members of distinct functional networks, and should be uncorrelated with each other.

This hypothesis is supported by the present fc-DOT imaging results. The stimuli resulted in symmetric functional responses. Then, with resting-state analysis, we saw high correlations bilaterally in the same regions as the task-related responses. The correlation maps are slightly broader than the task-response maps. This difference may be due to association with brain regions involved with higher-order processing; while these regions might not respond as strongly to the simple task paradigms, they may still correlate strongly in the resting-state. Additionally, the sensitivity of DOT imaging is lower near the pad edges, but the correlation analysis normalizes out differences in contrast, allowing the correlation maps to extend more fully to the margins of the field-of-view. Other interesting features in the visual cortex images were the lower correlation along the midline (where we expect the superior sagittal sinus) and the flat region of low correlation along the bottom of the imaging domain (cerebellum, which should be uncorrelated). Additionally, the fc-DOT maps showed low correlation between the two pads, demonstrating the expected independence of the two networks. Thus, these fc-DOT results produced the pattern predicted by fMRI and seen with our own subject-matched experiment.

Future fc-DOT studies will benefit from the use of stereotactic coordinates and atlases in order to align and combine multi-subject data. This could be accomplished with more precise registration of the imaging pads to anatomic landmarks (Gibson et al., 2003) followed by an affine transform to an atlas space, as in fMRI. It is worth noting, however, that the ability to make robust maps on single subjects, as demonstrated in this paper, is an essential step towards clinical neuroimaging, where a group-average image would be less helpful than a detailed scan of a particular patient.

In this study, we performed functional connectivity mapping using seed-based correlation analysis on image sequences band-pass filtered between 0.009 and 0.08 Hz. We chose this methodology in order to correspond to the processing stream in Fox et al. (2005); these particular filter limits remain common in fc-MRI processing (e.g., in Church et al., 2009). There are other methods for preprocessing functional connectivity data. For example, Zhang et al. and He et al. remove linear trends and use a 0.1 Hz low-pass filter while continuing to use seed-based correlation analysis (Zhang et al., 2008; He et al., 2008). Furthermore, one could use independent component analysis (ICA) to discriminate networks without assumptions about seed locations (De Luca et al., 2006; Greicius et al., 2004; Damoiseaux et al., 2006; Fransson et al., 2007). Since DOT's sensitivity to vascular compartments and sampling of systemic hemodynamics differs from those of MRI, the evaluation of different processing methods within the context of fc-DOT deserves future study.

Both fc-MRI and fc-DOT must remove global confounds and nuisance signals. Differences in the sensitivity and field-of-view of the two methods led to different regression steps preceding computation of the functional connectivity maps. For fc-MRI, the processing included regressions of the global signal, the white matter signal, and the ventricular signal. In contrast, DOT has only limited depth sensitivity and is unlikely to suffer artifacts from white matter and the ventricles. However, DOT measurements will be corrupted by hemodynamics in the scalp and skull as well as by slow global fluctuations due to auto-regulation (Franceschini et al., 2006; Obrig et al., 2000). To remove these confounds, we regressed out a signal derived from superficial measurements. This signal contains systemic hemodynamic variations as well as physiology located within the scalp and skull. This method increases the brain-specificity of the DOT method and permits the functional connectivity analysis of local cerebral hemodynamics.

Recently, controversy has surrounded the effects of systemic respiratory and cardiac variations on fc-MRI networks (Birn et al., 2008; Shmueli et al., 2007). While we believe that these artifacts have only small effects on fc-MRI mapping, the widespread adoption of functional connectivity techniques will be aided if the mechanisms, relationships, and strengths of different spontaneous signals were better understood. Cardiac and breathing pulsations affect resting-state measurements due to fMRI's low temporal sampling rate (a typical repetition time (TR) is 2.5 s), which causes high-frequency systemic physiology to be aliased into the low-frequency regime in an uncontrolled manner (Lowe et al., 1998). In contrast, our DOT system images its entire field-of-view every 93 ms, meaning that the carrier frequencies for cardiac and respiratory variations are unlikely to be aliased into lower-frequency bands where the functional connectivity signal is found and can be removed with simple low-pass filters. Thus, the RSNs found with fc-DOT can be more confidently ascribed to be free of aliasing artifacts.

There were small differences between correlation maps determined with different hemodynamic contrasts: the functional correlations were strong in ΔHbO_2 and ΔHbR, but noisier and less localized with ΔHbT. Since DOT instrument noise appears in the absorption measurements at each wavelength and physiologic noise appears in cerebral blood volume (CBV) and oxygen saturation (S_tO_2), with these preliminary results, the propagation of noise into the different contrasts is complicated. Future studies will be required to make physiologic judgments about the origins of these mapping differences.

The ability of discover maps in all three contrasts offers opportunities beyond those of BOLD-fMRI. Previous stimulus-response studies have found differences between images from the three contrasts, usually showing advantages to ΔHbT for functional mapping, including a tighter correlation to cerebral blood flow (CBF) and potentially better spatial localization (Devor et al., 2005; Culver et al., 2005; Sheth et al., 2004). While BOLD is primarily venous sensitive, each optical contrast can have different compartmental sensitivity (Dunn et al., 2005). In addition, while fc-MRI maps (primarily dependent on HbR) could have been due to fluctuations in either CBV or S_tO_2, our results show that maps are present in both CBV and S_tO_2. Our fc-DOT methods can in principal be extended to laser speckle measures of CBF, and future systems could provide simultaneous assessment of CBF, oxygen extraction fraction, and cerebral metabolic rate of oxygen consumption (Culver et al., 2003; Durduran et al., 2004; Dunn et al., 2005). Non-invasive optical techniques can also be combined with direct

measurements of systemic physiology, such as pulse and respiration rates and blood pressure, as was performed by Franceschini et al. (2006). While, in this paper, we removed systemic fluctuations in order to improve local neuronal specificity, Franceschini et al. showed that correlations to physiologic measurements can reveal information such as the flow of blood pressure waves through the circulation. Due to DOT's high sampling rate, similar analysis can be performed at higher frequencies (e.g., at the respiration and pulse rates). Future studies that evaluate these systemic physiologic correlation maps, in combination with the functional connectivity methods demonstrated herein, could help elucidate the effect of the vascular tree on resting-state signals. DOT also does not interfere with electrical recording techniques (Devor et al., 2003), allowing studies that more directly compare resting-state neuronal and vascular activity than are currently possible (He et al., 2008). All of these techniques should allow fc-DOT to gain insight into the origins of the functional connectivity signal and to improve knowledge of extraneous sources of variance in optical and MRI studies.

These results demonstrate the successful application of functional connectivity methods to DOT of adult human subjects. New high-density DOT systems may offer the resolution, signal-to-noise, and system simplicity that allow optical imaging to successfully translate to widespread use. Our results validate DOT functional connectivity methods (fc-DOT) within a model system established by fMRI. Such an approach increases our confidence in the fidelity of fc-DOT, providing a strong foundation for moving RSN analysis beyond the studies that fMRI is capable of performing. We look forward to extending the fc-DOT methods presented here to study questions of interest in contemporary neuroscience in the areas of brain disease, development, and physiology.

Acknowledgments

We thank Benjamin Zeff, Gavin Perry, and Martin Olevitch for help with DOT instrumentation and software; Russ Hornbeck, John Harwell, and Donna Dierker for help with Caret; and Benjamin Zeff for helpful comments on the manuscript. This work was supported in part by NIH grants R21-EB007924, R21-HD057512 (J.P.C.), T90-DA022871 (B.R.W.), P50-NS06833 (M.E.R. and A.Z.S.), K02-NS053425 (B.L.S), R01-NS46424 (S.E.P.), and 1F30NS062489 (A.L.C.) and NSF grant 0548890 (A.LC.).

References

Birn, R.M., Murphy, K., et al., 2008. The effect of respiration variations on independent component analysis results of resting state functional connectivity. Hum. Brain Mapp. 29, 740–750.
Biswal, B., Yetkin, F.Z., et al., 1995. Functional connectivity in the motor cortex of resting human brain using echo-planar MRI. Magn. Reson. Med. 34, 537–541.
Bluestone, A.Y., Abdoulaev, G., et al., 2001. Three-dimensional optical tomography of hemodynamics in the human head. Opt. Express 9, 272–286.
Boden, S., Obrig, H., et al., 2007. The oxygenation response to functional stimulation: is there a physiological meaning to the lag between parameters? NeuroImage 36, 100–107.
Bonakdarpour, B., Parrish, T.B., et al., 2007. Hemodynamic response function in patients with stroke-induced aphasia: implications for fMRI data analysis. NeuroImage 36, 322–331.
Born, P., Leth, H., et al., 1998. Visual activation in infants and young children studied by functional magnetic resonance imaging. Pediatr. Res. 44, 578–583.
Church, J.A., Fair, D.A., et al., 2009. Control networks in paediatric Tourette syndrome show immature and anomalous patterns of functional connectivity. Brain 132, 225–238.
Colonnese, M.T., Phillips, M.A., et al., 2008. Development of hemodynamic responses and functional connectivity in rat somatosensory cortex. Nat. Neurosci. 11, 72–79.
Culver, J.P., Durduran, T., et al., 2003. Diffuse optical tomography of cerebral blood flow, oxygenation and metabolism in rat during focal ischemia. J. Cereb. Blood Flow Metab. 23, 911–923.
Culver, J.P., Siegel, A.M., et al., 2005. Evidence that cerebral blood volume can provide brain activation maps with better spatial resolution than deoxygenated hemoglobin. NeuroImage 27, 947–959.
D'Esposito, M., Deouell, L.Y., et al., 2003. Alterations in the bold fMRI signal with ageing and disease: a challenge for neuroimaging. Nat. Rev. Neurosci. 4, 863–872.
Damoiseaux, J.S., Rombouts, S.A.R.B., et al., 2006. Consistent resting-state networks across healthy subjects. Proc. Natl. Acad. Sci. U. S. A. 103, 13848–13853.
De Luca, M., Beckmann, C.F., et, al., 2006. fMRI resting state networks define distinct modes of long-distance interactions in the human brain. NeuroImage 29, 1359–1367.
Dehghani, H., Pogue, B.W., et al., 2003. Multiwavelength three-dimensional near-infrared tomography of the breast: initial simulation, phantom, and clinical results. Appl. Opt. 42, 135–145.
Devor, A., Dunn, A.K., et al., 2003. Coupling of total hemoglobin concentration, oxygenation, and neural activity in rat somatosensory cortex. Neuron 39, 353–359.
Devor, A., Ulbert, I., et al., 2005. Coulping of the cortical hemodynamic response to cortical and thalamic neuronal activity. Proc. Natl. Acad. Sci. U. S. A. 102, 3822–3827.
Dunn, A.K., Devor, A., et al., 2005. Spatial extent of oxygen metabolism and hemodynamic changes during functional activation of the rat somatosensory cortex. NeuroImage 27, 279–290.
Durduran, T., Yu, G., et al., 2004. Diffuse optical measurement of blood flow, blood oxygenation, and metabolism in a human brain during sensorimotor cortex activation. Opt. Lett. 29, 1766–1768.
Elwell, C.E., Springett, R., et al., 1999. Oscillations in cerebral haemodynamics—Implications for functional activation studies. In: Eke, A., Delpy, D. (Eds.), Oxygen Transport to Tissue XXI. Kluwer Academic / Plenum Publishers, New York, pp. 57–65.
Fair, D.A., Dosenbach, N.U.F., et al., 2007. Development of distinct control networks through segregation and integration. Proc. Natl. Acad. Sci. U. S. A. 104, 13507–13512.
Fair, D.A., Cohen, A.L., et al., 2008. The maturing architecture of the brain's default network. Proc. Natl. Acad. Sci. U. S. A. 105, 4028–4032.
Fox, M.D., Raichle, M.E., 2007. Spontaneous fluctuations in brain activity observed with functional magnetic resonance imaging. Nat. Rev,. Neurosci. 8, 700–711.
Fox, M.D., Snyder, A.Z., et al., 2005. The human brain is intrinsically organized into dynamic, anticorrelated functional networks. Proc. Natl. Acad. Sci. U. S. A. 102, 9673–9678.
Franceschini, M.A., Joseph, D.K., et al., 2006. Diffuse optical imaging of the whole head. J. Biomed. Opt. 11, 054007.
Fransson, P., Skiold, B., et al., 2007. Resting-state networks in the infant brain. Proc. Natl. Acad. Sci. U. S. A. 104, 15531–15536.
Fujiwara, N., Sakatani, K., et al., 2004. Evoked-cerebral blood oxygenation changes in false-negative activations in BOLD contrast functional MRI of patients with brain tumors. NeuroImage 21, 1464–1471.
Gibson, A.P., Riley, J., et al., 2003. A method for generating patient-specific finite element meshes for head modelling. Phys. Med. Biol. 48, 481–495.
Gibson, A.P., Austin, T., et al., 2006. Three-dimensional whole-head optical tomography of passive motor evoked responses in the neonate. NeuroImage 30, 521–528.
Greicius, M.D., Srivastava, G., et al., 2004. Default-mode network activity distinguishes Alzheimer's disease from healthy aging: evidence from functional MRI. Proc. Natl. Acad. Sci. U. S. A. 101, 4637–4642.
Greicius, M.D., Flores, B.H., et al., 2007. Resting-state functional connectivity in major depression: abnormally increased contributions from subgenual cingulate cortex and thalamus. Biol. Psychiatry 62, 426–437.
He, B.J., Snyder, A.Z., et al., 2008. Electrophysiological correlates of the brain's intrinsic large-scale functional architecture. Proc. Natl. Acad. Sci. U. S. A. 105, 16039–16044.
Heeger, D.J., Ress, D., 2002. What does fMRI tell us about neuronal activity? Nat. Rev. Neurosci. 3, 142–151.
Iadecola, C., 2004. Neurovascular regulation in the normal brain and in Alzheimer's disease. Nat. Rev., Neurosci. 5, 347–360.
Jasdzewski, G., Strangman, G., et al., 2003. Differences in the hemodynamic response to event-related motor and visual paradigms as measured by near-infrared spectroscopy. NeuroImage 20, 479–488.
Joseph, D.K., Huppert, T.J., et al., 2006. Diffuse optical tomography system to image brain activation with improved spatial resolution and validation with functional magnetic resonance imaging. Appl. Opt. 45, 8142–8151.
Katura, T., Tanaka, N., et al., 2006. Quantitative evaluation of interrelations between spontaneous low-frequency oscillations in cerebral hemodynamics and systemic cardiovascular dynamics. NeuroImage 31, 1593–1600.
Lowe, M.J., Mock, B.J., et al., 1998. Functional connectivity in single and multislice echoplanar imaging using resting-state fluctuations. NeuroImage 7, 119–132.
Morita, T., Kochiyama, T., et al., 2000. Difference in the metabolic response to photic stimulation of the lateral geniculate nucleus and the primary visual cortex of infants: a fMRI study. Neurosci. Res. 38, 63–70.
Obrig, H., Neufang, M., et al., 2000. Spontaneous low frequency oscillations of cerebral hemodynamics and metabolism in human adults. NeuroImage 12, 623–639.
Obrig, H., Villringer, A., 2003. Beyond the visible—Imaging the human brain with light. J. Cereb. Blood Flow Metab. 23, 1–18.
Raichle, M.E., Mintun, M.A., 2006. Brain work and brain imaging. Annu. Rev. Neurosci. 29, 449–476.
Reinhard, M., Wehrle-Wieland, E., et al., 2006. Oscillatory cerebral hemodynamics—the macro - vs. the microvascular level. J. Neurol. Sci. 250, 103–109.
Rowley, A.B., Payne, S.J., et al., 2007. Synchronization between arterial blood pressure and cerebral oxyhaemoglobin concentration investigated by wavelet cross-correlation. Physiol. Meas. 28, 161–173.
Saager, R.B., Berger, A.J., 2005. Direct characterization and removal of interfering absorption trends in two-layer turbid media. J. Opt. Soc. Am. A. 22, 1874–1882.
Schroeter, M.L., Bucheler, M.M., et al., 2005. Spontaneous slow hemodynamic oscillations are impaired in cerebral microangiopathy. J. Cereb. Blood Flow Metab. 25, 1675–1684.

Sheth, S.A., Nemoto, M., et al., 2004. Columnar specificity of microvascular oxygenation and volume responses: implications for functional brain mapping. J. Neurosci. 24, 634–641.
Shmueli, K., van Gelderen, P., et al., 2007. Low-frequency fluctuations in the cardiac rate as a source of variance in the resting-state fMRI BOLD signal. NeuroImage 38, 306–320.
Steinbrink, J., Villringer, A., et al., 2006. Illuminating the BOLD signal: combined fMRI-fNIRS studies. Magn. Reson. Imaging 24, 495–505.
Van Essen, D.C., Drury, H.A., et al., 2001. An integrated software suite for surface-based analyses of cerebral cortex. J. Am. Med. Inform. Assoc. 8, 443–459.
Yodh, A., Chance, B., 1995. Spectroscopy and imaging with diffusing light. Physics Today 48, 34–40.
Zeff, B.W., White, B.R., et al., 2007. Retinotopic mapping of adult human visual cortex with high-density diffuse optical tomography. Proc. Natl. Acad. Sci. U. S. A. 104, 12169–12174.
Zhang, D., Snyder, A.Z., et al., 2008. Intrinsic functional relations between human cerebral cortex and thalamus. J. Neurophysiol. 100, 1740–1748.
Zou, P., Mulhern, R.K., et al., 2005. BOLD responses to visual stimulation in survivors of childhood cancer. NeuroImage 24, 61–69.